Proceedings of the Canadian Society for Mechanical Engineering International Congress 2022
CSME Congress 2022
June 5-8, 2022, Edmonton, AB, Canada

EXPERIMENTAL ANALYZES OF CAPSULES' BEHAVIOUR IN A CURVED MICROCHANNEL

Yeganeh Saffar[1], David S. Nobes[1], Reza Sabbagh[1*]
[1]Mechanical Engineering Department, University of Alberta, Edmonton, Canada
* Reza.Sabbagh@ualberta.ca

Abstract— The interaction between a capsule (bubble or droplet) and a flow structure of the continuous phase can affect the properties of the liquids, cells, and particles transferring within the capsule. Channel geometry is a common example of the flow structure influencer. Investigating the effect of Dean vortices on the capsule trajectory and top view topology helps to understand the effect of such geometries on the content of the capsules. The effect of curvature length on the capsule shape and trajectory is studied as the azimuthal angle in high continuous phase flow rates. Capsules are generated from a 2-propanol-water mixture with a broad range of diameters 50 (μm) $\leq d \leq$ 1000 (μm) in a microchannel with a 270° curvature. Experimental results and image processing schemes provide information on the variation of deformation index (DI) as well as the length and the width of the capsule. It has been shown that when the capsule passes through the curved channel, it migrates from the outer half of the channel toward the inner half. The length of the capsule experiences two peaks with 37% increase in comparison to its starting value through the channel. The width of the capsule is observed to have a reverse relation with the length.

Keywords-component; capsule deformation; microfluidics; curved channel

I. INTRODUCTION

Immiscible liquid-liquid microfluidics has gained extensive attention due to its various applications such as diagnostics for circulating cancer cells [1] and malaria-infected red blood cells [2], targeted drug delivery when passing through complex geometry vessels [3], cosmetics, and food [4] and chemical reactions [5]. Capsules (bubbles or droplets) passing through curved geometries can be affected by the lateral movement of the flow induced by the pressure gradient across the width of the channel [6]. The lateral motion of the flow usually forms two or four counter-rotating Dean vortices [6]. The interaction between a capsule and the Dean vortices introduces capsule deformation and trajectory deviation [7].

The interaction between the capsules and the fluid structures has been extensively studied in straight channels and capillaries both experimentally and numerically [7] [8]. The study of the shear module of the thin-walled capsules [9] and the flow structure inside them [10] are some examples of investigations in such channels. Other complex geometries such as a T-junction [11] and multiple branch channels [12] have been recently studied. Geometrical properties and dynamics of the capsules in the curved channels have been studied numerically in a 180° and a donut shape channel [8]. In which continuous and dispersed phased are considered similar but immiscible. These similarities found in the simulation are not consistent with experimental findings in most cases [8].

The aim of this work is to study the deformation and migration of immiscible capsules with different viscosity fluids experimentally. For this purpose, a microchannel is designed as simplified curved vessels to simulate the effect of curved geometry. A custom-made image processing algorithm is used to capture the capsule topology and centroid. Using this information, the trajectory and topology of the capsules are studied in the presence of Dean vortices.

II. METHOD

A. Capsule generation

The immiscible capsules generated using a 2-propane-water mixture with concentration, c of $0\% \leq c \leq 80\%$. A variation of capsule sizes with the equivalent diameter of 50 (μm) $\leq d \leq$ 1000 (μm) is used for the investigation. To obtain the required capsules' diameters, a flow-focusing droplet generator (DG) is employed due to its wide range of droplet size, generation rate, and lower droplet size variation coefficient [13]. The droplet generator is designed using a web-based tool, DAFD [14] that uses machine learning algorithms to automate the design of flow-focusing droplet generators. The mean absolute error of the droplet diameter range in this design is less than 10 (μm) [14].

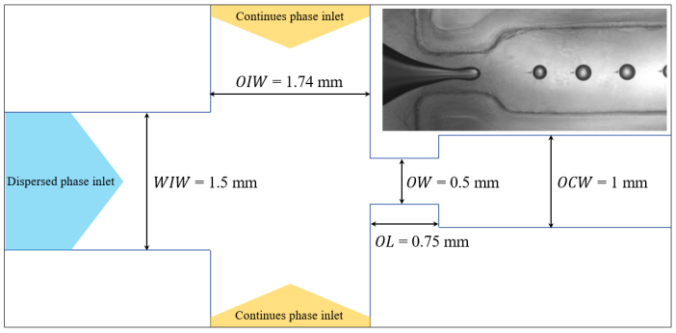

WIW	*OIW*	*OW*	*OL*	*OCW*
Water inlet width	Oil inlet width	Orifice width	Orifice length	Outlet channel width

Figure 1. Schematics of the flow-focusing droplet generator employed to generate water droplets in the oil medium and an image of the generated droplets (top right).

Figure 1 shows a map of the droplet generator with a real-time image of the generated droplets and defines the main parameters in a droplet generator design. The *OCW* is chosen equal to the experimental microchannel with a square cross-section with width, w = 1 (mm). Canola oil, as the continuous phase, enters the droplet generator from the sides and the 2-propanol-water mixture enters the middle entrance as the dispersed phase. Monodispersed capsules in both dripping and jetting regime are generated by this device.

B. *Microchannel Design*

The microchannel shown in Figure 2 has been designed with a 270° curved geometry to increase the capsule travel duration in the curvature. It contains droplet generator, settling channel, and a curved section with a radius of curvature, r = 3.5 (mm), and the channel width is w = 1 (mm). Capsules transfer from the droplet generator outlet and pass through a straight section (settling channel) with a length, $25\times w \leq L$ ensuring the stabilization of the capsules before entering the curved section.

The flow cell and its connection to the optical table are printed using a SLA 3D printer (Form 3, FormLab Inc.) using the semi-transparent resin to have optical access to the channel. The optical window that is attached to the top of the flow channels is made using a laser cutter from an acrylic sheet with a thickness of 6.35 (mm). An elastic membrane, silicone sheet with thickness of 0.5 (mm), and Shore A hardness of 60±5 is used between flow the channel and optical window to seal the flow cell.

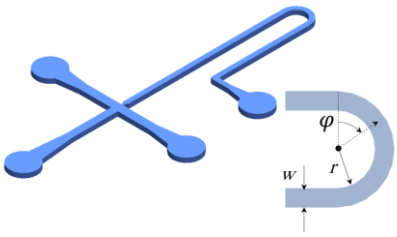

Figure 2. Microchannel with a flow-focusing droplet generator and a 270° curved section with aradius of curvature of 3.5 (mm) and width of 1 (mm).

C. *Experimental setup*

Figure 3 shows the experimental setup used to image the motion of the capsules. The setup contains an optical and a fluid system. In the optical system, a compact high intensity spot LED light (SL191, Advanced Illumination) is employed as a backlight illuminator. Capsules are captured by a high frame rate camera (BASLER) of 200 (fps). A macro lens is attached to the camera to provide a 6.5 (mm)×9 (mm) field of view. The fluid system contains two programmable syringe pumps (PHD4400, Harvard Apparatus) used for both the 2-propane-water mixture as the dispersed phase and canola oil as the continuous phase.

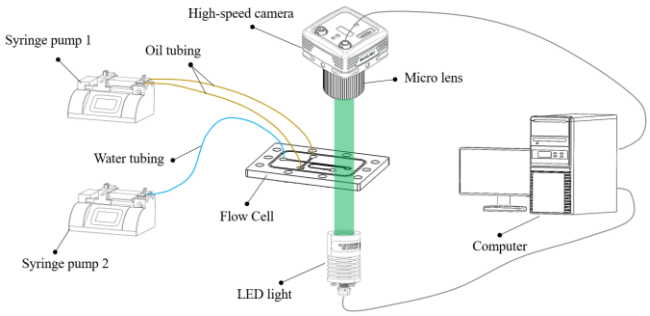

Figure 3. The schematic of the experimental setup containing optical and fluid systems designed to implement shadowgraph imaging technique.

D. *Image processing*

A custom-made image processing scheme is developed in MATLAB to follow the capsules in channels. Figure 4 (a) shows the combination of 17 successive frames of a capsule passing through the microchannel with the flow rate of 60 ml/h. Figure 4 (b) shows the binarized image resulting from a combination of a sequence of raw images in Figure 4 (a). For each capsule, the centroid from the projected area of the image is located and the azimuthal angle of the capsule location is determined with respect to this point. From the binary images, capsule area and boundary points are extracted for further investigations.

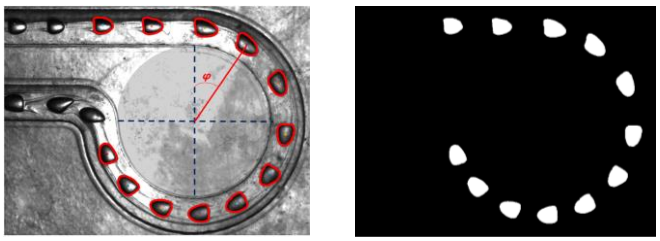

(a) (b)

Figure 4. (a) The combination of 17 successive frames of a capsule passing through channel with the flow rate of 60 (ml/h). (b) The processed image used to extract capsule properties for a capsule passing through channel.

III. RESULTS AND DISCUSSION

A. *Capsule migration*

A typical trajectory of a single capsule centroid passing through a curved channel in comparison to the center of the channel is shown in Figure 5. The equivalent diameter of the

capsule is d = 500 (μm) and the continuous phase flow rate is 45 (ml/h). The capsule is generated from a mixture of 20% 2-propane and 80% water. The distance between the centroid of the capsule and the centerline of the channel divided by the channel half width (w/2) is measured as the deviation shown in absolute quantity. In the settling section (φ < 0°), the capsule is migrating with less than 2% deviation of its centroid from the center of the channel. Entering the curvature, the capsule moves slightly to the outer half of the channel with 6% deviation of centroid from the channel centerline. As can be seen in Figure 5, deviation decreases as capsule moves through channel and φ increases. At φ = 90° its centroid passes the centerline and deviation increases on the inner half of the channel. Near the curvature, outlet deviation is its maximum amount equal to 10%. It is also shown that the variations in the deviation with increasing the azimuthal angle follows a linear trend on both sides of the centerline.

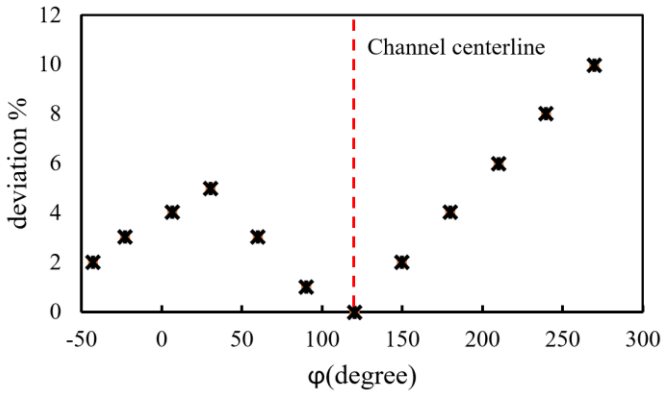

Figure 5. Capsule deviation in channel B with a continuous phase flow rate of 45 (ml/h).

The locations of the capsule leading edge, L.E. are shown in Figure 6 at two different azimuthal angles. It is compared to the location of the centerline intersecting with the capsule boundary using the capsule centroid as the reference. Figure 6 (a) shows the capsule at φ = 100°, the L.E., and the centroid both are leaning toward the concave wall. As the capsule moves forward the L.E. point shifts toward the convex wall as it is shown in Figure 6(b) where φ = 210° and the L.E. point is detected in the inner half of the channel.

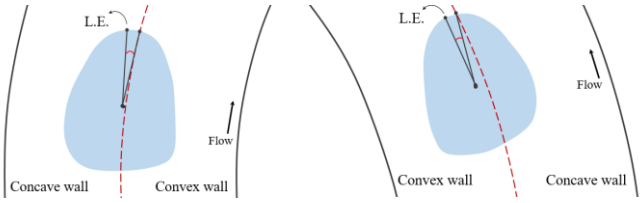

(a) (b)

Figure 6. The leading edge deviation angle, θ for a capsule at two different positions (a) φ = 100° and (b) φ = 210° with continuous phase flow rate of 45 (ml/h).

B. *Capsule deformation*

The deformation of a single capsule from its original circular projected shape is studied using its properties explained in Figure 7 such as length, L_d, width, W_d, and deformation Index, *DI*. The largest and smallest distances (L_{max} ,L_{min}) between the edges of the capsule and its centroid are used to calculate the deformation index, *DI*, as:

$$DI = \frac{L_{max} - L_{min}}{L_{max} + L_{min}} \qquad \text{Equation 1}$$

with a range of $0 \leq DI < 1$ where zero refers to a spherical capsule with constant diameter in a 2D plane. The azimuthal angle, φ, and capsule path radius, r_d are shown in Figure 7.

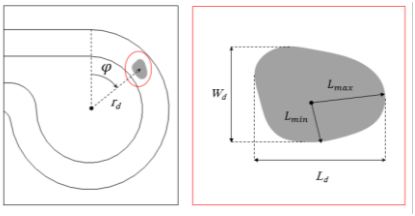

Figure 7. The schematic of capsule properties and its azimuthal location in the channel.

As the capsule moves forward through the channel the deformation is observable in changes of both maximum length, L_d and maximum width, W_d of the capsule. Figure 8 shows the variation of L_d for 3 different capsules with equivalent diameters of 600, 700, and 800 (μm), D1, D2, D3,respectively, passing through channel with continuous phase flow rate of 45 (ml/h). For example, the 800 (μm) capsule (D3) stretches after entering the channel to 37% at P1 around φ = 70°. It shrinks to its starting length at P2 where φ = 180° and increases once more before the outlet of the curvature at P3. The same behavior is observable for the smaller capsules, however, the variation of capsule length decreases as the capsule equivalent diameter decreases.

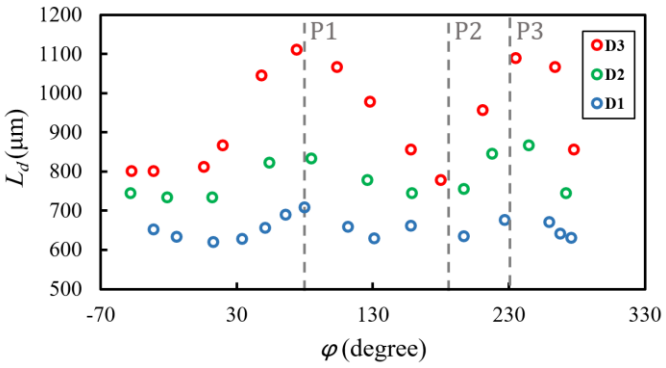

Figure 8. Variation of capsule length for 3 different capsules with d=[600 (D1),700 (D2),800 (D3)] (μm).

The maximum width of the capsule changes with a relation to its length. The variation of W_d is presented in Figure 9 for capsules with d = [600 (D1), 700 (D2),800 (D3)] (μm). As the capsule enters the channel its length starts to shrink for about 38% with a minimum point around φ = 70° which is the

maximum point of L_d variations. Moving forward, the width of the capsule increases first and then decreases near the end of the curvature. A similar behavior is observed for smaller capsules and can be seen in Figure 9. The width shrinking decreases as the capsule's equivalent diameter reduces from 800 (μm) to 600 (μm). For the smaller capsules the width slightly decreases and then the major increase appears in the range of $110° \leq \varphi \leq 190°$.

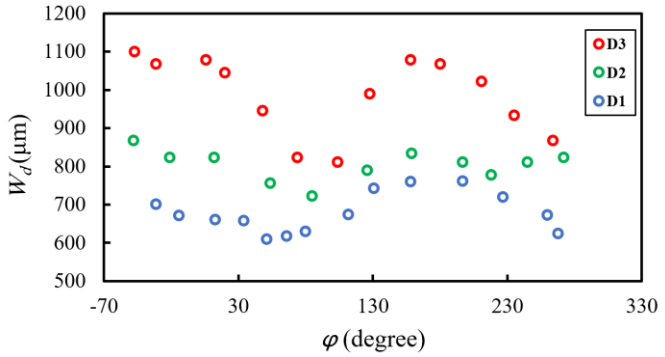

Figure 9. Variation of capsule width for 3 different capsules with d=[600,700,800] (μm).

The deformation of a capsule with d = 550 (μm) is presented in Figure 10 using iso-surface to connect its boundary at different angles to visualized the orientation changes. It is shown in Figure 10 (a) that a major increase in the capsule length happens near the entrance of the curvature where the lateral flow movements start. The capsule width is almost constant with a slight increase of 10% through the channel as shown in Figure 10 (b). Considering the capsule is immiscible in the flow and has a constant volume, a 30% changes in length with a constant width results in a sudden reduction of about the $\varphi = 34^{o}$ in the capsule depth.

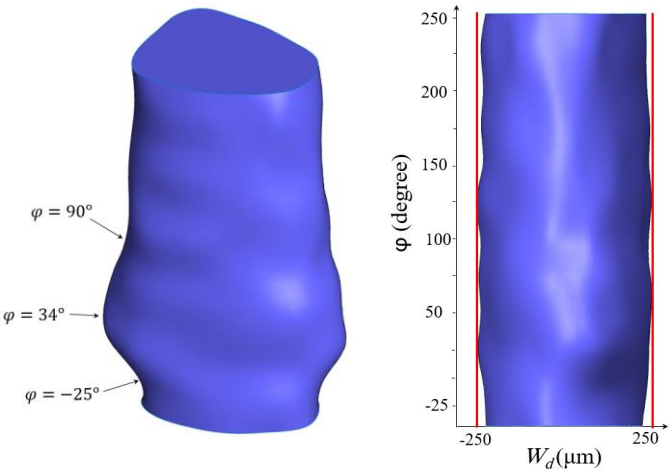

(a) (a)

Figure 10. The deformation of a capsule with d= 550 (μm) with continuous phase flow rate of 45(ml/h).

IV. Conclusion

An experiment was conducted to study the capsule topology and trajectory in a square ccross-sectioncurved geometry with 1 (mm) width. It is shown that there is a reverse relation between length and width of the capsule. It is also presented that length and width both experience 40% change of value through the channel. It is shown that capsules migrate from the outer half to the inner half microchannel while traversing a long radius bend.

References

[1] J. Guck, S. Schinkinger, B. Lincoln, F. Wottawah, and S. Ebert, *et al*, "Optical deformability as an inherent cell marker for testing malignant transformation and metastatic competence," *Biophys. J.*, vol. 88, no. 5, pp. 3689–3698, 2005, doi: 10.1529/biophysj.104.045476.

[2] H. Bow, I. V. Pivkin, M. Diez-Silva, S. J. Goldfless, and M. Dao, *et al*, "A microfabricated deformability-based flow cytometer with application to malaria," *Lab Chip*, vol. 11, no. 6, pp. 1065–1073, 2011, doi: 10.1039/c0lc00472c.

[3] M. Abkarian, M. Faivre, R. Horton, K. Smistrup, C. A. Best-Popescu, and H. A. Stone, "Cellular-scale hydrodynamics," *Biomed. Mater.*, vol. 3, no. 3, 2008, doi: 10.1088/1748-6041/3/3/034011.

[4] M. P. Neubauer, M. Poehlmann, and A. Fery, "Microcapsule mechanics: From stability to function," *Adv. Colloid Interface Sci.*, vol. 207, no. 1, pp. 65–80, 2014, doi: 10.1016/j.cis.2013.11.016.

[5] A. Lafzi, A. H. Raffiee, and S. Dabiri, "Inertial migration of a deformable capsule in an oscillatory flow in a microchannel," *Phys. Rev. E*, vol. 102, no. 6, pp. 1–9, 2020, doi: 10.1103/PhysRevE.102.063110.

[6] N. Nivedita, P. Ligrani, and I. Papautsky, "Dean flow dynamics in low-aspect ratio spiral microchannels," *Sci. Rep.*, vol. 7, no. October 2016, pp. 1–10, 2017, doi: 10.1038/srep44072.

[7] S. Ebrahimi, P. Balogh, and P. Bagchi, "Motion of a capsule in a curved tube," *J. Fluid Mech.*, 2020, doi: 10.1017/jfm.2020.831.

[8] E. Häner, M. Heil, and A. Juel, "Deformation and sorting of capsules in a T-junction," *J. Fluid Mech.*, 2019, doi: 10.1017/jfm.2019.979.

[9] L. Zhu and L. Brandt, "The motion of a deforming capsule through a corner," *J. Fluid Mech.*, vol. 770, pp. 374–397, 2015, doi: 10.1017/jfm.2015.157.

[10] C. Yan, "Flow topology and its transformation inside droplets traveling in rectangular microchannels," *Phys. Fluids*, vol. 32, no. 5, p. 052009, 2020, doi: 10.1063/5.0004549.

[11] S. B. Q. Tran, Q. T. Le, F. Y. Leong, and D. V. Le, "Modeling deformable capsules in viscous flow using immersed boundary method," *Phys. Fluids*, vol. 32, no. 9, 2020, doi: 10.1063/5.0016302.

[12] S. B. Q. Tran, Q. T. Le, F. Y. Leong, and D. V. Le, "Modeling deformable capsules in viscous flow using immersed boundary method," *Phys. Fluids*, vol. 32, no. 9, pp. 1–12, 2020, doi: 10.1063/5.0016302.

[13] A. Lashkaripour, C. Rodriguez, L. Ortiz, and D. Densmore, "Performance tuning of microfluidic flow-focusing droplet generators," *Lab Chip*, vol. 19, no. 6, pp. 1041–1053, 2019, doi: 10.1039/C8LC01253A.

[14] A. Lashkaripour, C. Rodriguez, N. Mehdipour, R. Mardian, and D. McIntyre, *et al*, "Machine learning enables design automation of microfluidic flow-focusing droplet generation," *Nat. Commun.*, vol. 12, no. 1, 2021, doi: 10.1038/s41467-020-20284-z.